Research Article **Open Access**

N. Sánchez Castro, M. A. Palomino-Ovando, D. Estrada-Wiese, J. A. del Río, M. B. de la Mora, R. Doti, J. Faubert, and J. E. Lugo*

A photonic self-oscillator based on porous silicon

DOI 10.1515/mesbi-2016-0003
Received April 1, 2016; revised July 2, 2016; accepted July 5, 2016

Abstract: We induced mechanical self-oscillations in a microcavity structure made of porous silicon one-dimensional photonic crystals (PSi-1DPC) with an air gap. The electromagnetic force generated within the whole photonic structure, by light with a wavelength of 633 nm, is enough to overcome energy losses and sustain self-oscillations. From these mechano-optical measurements we estimated the stiffness and Young's modulus of porous silicon and compared the results with values reported elsewhere and with values estimated herein by a mechanical method. We obtained good agreement between all values.

Keywords: photonic crystal; auto-oscillation; self-oscillator; porous silicon

1 Introduction

Porous silicon (PSi) is an interesting optical material that has been investigated intensively for many decades. Originally the most attractive property of PSi was its room-temperature luminescence and the possibility of building light emitting diode devices. Most of the PSi applications are found in the field of sensing [1] and communications [2] where photonic crystals (PCs) has been used as either the active sensing structure or as selective filter.

Photonic crystals are normally made of periodic dielectric materials [3] sometimes nanostructures [4] that alter the propagation of photons. Photons circulate through this structure depending on their wavelength. Wavelengths that are granted to pass are known as modes and theses groups of modes form photonic bands. Banned bands of wavelengths are known as photonic bandgaps. Photonic crystals give rise to different optical phenomena such as high-reflecting omni-directional mirrors [5], Bloch oscillations [6, 7], sensing [8], negative refraction [9], and Mechanical oscillations: forced-oscillations and self-oscillations [10, 11].

Self-oscillation [12] is defined as the generation and maintenance of a periodic motion by a source of power that lacks a corresponding periodicity. That is, in a system, the oscillation itself controls the phase with which the power source acts on it [13]. Self-oscillators are distinct from resonant systems (including both forced and parametric resonators), in which the oscillation is driven by a source of power that is modulated externally. The self-oscillation is itself an interesting phenomenon because many types of systems can self-oscillate. For instance, cardiac cells [14], likewise the firing of certain kind of neurons, ocean waves, and the pulsation of variable stars, human voice, and some business cycles are self-oscillatory [15]. Furthermore, self-oscillation has long been an essential aspect of human technology. The phenomenon has been analyzed and used in the development of technology: the mechanism of clocks, turbines, musical instruments (violin and pipe organs), heat engines, and lasers are self-oscillators. Yoshida, for example reported to have developed gels with an autonomous self-oscillating function like a heart muscle [16, 17].

In the past we have studied mechanical self and forced oscillations induced by electromagnetic forces. In [10] a microcavity made of two PSi-1DPC with an air defect, surface area of 8 mm^2 self-oscillate at a frequency of 16 Hz when a laser power level of 13 mW impinged over the microcavity at angle of 35 degrees. The self-oscillation allowed formulate a mathematical model that described forced oscillations at 9 Hz as well. In [11] more experi-

N. Sánchez Castro, M. A. Palomino-Ovando: Benemérita Universidad Autónoma de Puebla, Physics and Mathematics Sciences Department, Av. San Claudio y Río Verde, Col. San Manuel, Puebla, 72570, Mexico, E-mail: n_mex@outlook.com
D. Estrada-Wiese, J. A. del Rıo: Instituto de Energías Renovables, Universidad Nacional Autonóma de México. Privada Xochicalco S/N, 62580 Temixco, Morelos, Mexico, E-mail: de.e.wiese@gmail.com, arp@ier.unam.mx
M. B. de la Mora: CCADET Universidad Nacional Autónoma de México. Circuito Exterior S/N 04510 Ciudad de México, México
R. Doti, J. Faubert: Université de Montréal, Visual Psychophysics and Perception Laboratory, School of Optometry, Montreal H3C3J7, Canada
***Corresponding Author: J. E. Lugo:** Université de Montréal, Visual Psychophysics and Perception Laboratory, School of Optometry, Montreal H3C3J7, Canada, E-mail: eduardo.lugo@gmail.com

mental conditions were reported such as different forced frequencies and power levels. Theoretical electromagnetic force profiles for different optical power levels and defect lengths were calculated when light impinges with an angle of zero degrees. This calculation guided us finding optimal theoretical conditions where force values were highest. Predicted values were of the order of tenths to hundredths nN. Moreover the mathematical model developed in [10] was used to estimate the electromagnetic forces generated within the microcavity. Experimentally we found that for low frequencies at 8 mW the forces where of the same order of magnitude than the ones predicted by the model.

Herein we extended our previous study on self-oscillations of a microcavity made of two PSi-1DPC with an air-gap, surface area of 8 mm^2. A laser power level of 13 mW impinged over the microcavity at angle of 35 degrees and wavelength of 633 nm. FDTE simulations and mathematical calculations showed that under these experimental conditions there is no localized states formation. Nonetheless the electromagnetic force is enough to create more than one self-oscillation frequency. We explored under these experimental conditions how many self-oscillating frequencies were presented. In order to show that laser fluctuations or mechanical vibrations introduced by the setup, building or environment are not the self-oscillation origin, we tracked down laser power levels with a photocell and we measured mechanical oscillations from the photonic structure with and without laser light during 5 minutes. No oscillations whatsoever were obtained meaning that power fluctuations or any other mechanical vibrations do not create the condition for self-oscillations. In order to strengthen the conclusions we estimated the mechanical stiffness k and Young modulus by means of measuring the PSi-1DPC displacement δ when it was loaded with a known force. We compared these mechanical measurements with our opto-mechanical results and results from elsewhere and found good agreement between all results.

The work is organized as follows: first, in the experimental section we describe the methods and materials. Second, we present all the theoretical models and computer simulations used here. Third, in section fourth the results are described. Fourth, we discuss all the results and finally, we give some conclusions in section sixth.

2 Methods and materials

2.1 Sample preparation

PSi was fabricated by wet electrochemical etching of highly boron-doped c-Si substrates with orientation (100) and electrical resistivity of 0.001–0.005 Ohm-cm (room temperature= 25 °C, humidity=30%) [18]. On one side of the c-Si wafer, an aluminum film was deposited and then heated at 550 °C during 15 minutes in nitrogen atmosphere to produce a good electrical contact. An electrolyte composed of hydrofluoric acid, ethanol and glycerin in a ratio of 3:7:1 was used. In addition, the HF concentration was maintained constant during the etching process using a peristaltic pump to circulate the electrolyte within the Teflon^{TM} cell. To produce the PC, current density applied during the electrochemical dissolution was alternated from 40 mA/cm^2 (layer 1) to 3 mA/cm^2 (layer 2) and 10 periods (20 layers) were made. The current density conditions gave layers with porosities of 88% and 65% respectively. Free standing PSi-1DPCs were made at the end of the formation process by applying an anodic electropolishing current pulse (500 mA/cm^2 for 2 s). PSi samples were partially oxidized at 350 °C for 10 minutes. The best refractive index values we found that fit the experimental photonic bandgap structure (not shown) are $n_1 = 1.1$ and $n_2 = 2$. SEM images allowed measuring the thicknesses of each layer whose values were $d_1 = 326 \pm 11$ nm and $d_2 = 435 \pm 11$ nm. Fig. 1a shows a high resolution SEM picture of a PSi-1DPC cross section.

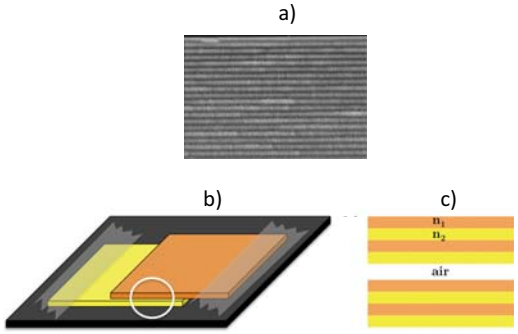

Figure 1: a) High resolution SEM image of a PSi-1D PC cross section. b) Schematic representation of the porous silicon microcavity structure. The first 1DPC (yellow) attached to the substrate with tape and the second 1DPC (orange) attached to the substrate with two pieces of tape overlapped. c) Representation of the photonic structure showing the multilayers (orange and yellow) and the air-gap that is the space (white) between the two 1DPCs.

2.2 Photonic structure

The photonic structure consisted of two PSi-1DPCs with an air gap between them. As the material is very fragile and delicate handling is needed. For that reason we choose the simplest possible configuration. We made 5 structures with similar physical characteristics. In Fig. 1b we show a simple sketch of this structure. Each PSi-1DPC had the following average dimensions: length $L = 4$ mm, width $b = 2$ mm, and thickness $t = 7.61\ \mu m$. Therefore the average surface area is $A = Lb = 8 \times 10^{-6}\ m^2$, the average volume $V = 6.09 \times 10^{-11}$ m^3. The volumetric density of each layer is the product of (1-P) × 2330 kg/m^3, where P means porosity. The value of 2330 kg/ m^3 corresponds to the volumetric density of c-Si. Since each PSi-1DPC contains two different porosities therefore there are two different volumetric densities. In order to obtain an effective volumetric density, we can take a weight average of both densities where the weights correspond to each thickness fraction. The final result is $\rho_{PSi-1DPC} = 586$ kg/m^3. Multiplying the volume times the effective volumetric density give us the average mass $m_{PSi-1DPC}$, which has a value of 3.57×10^{-8} kg.

2.3 Role of laser fluctuations or mechanical vibrations introduced by external factors on self-oscillations origin

First, we mounted the structure on a rotary and XY linear stages and all external vibrations induced on the structure were measured with the vibration meter for 5 minutes. Second, TE polarized laser red light impinged at 35 degrees on the microcavity (13 mW power level) for another 5 minutes and again we measured all external vibrations induced on the structure. Third, the Power Spectrum Density (PSD) of the signal was calculated. Moreover by using an oscilloscope and a photocell, we verified the light signal waveform and duty cycle after the light beam was chopped. This control helped to compare the light signal waveform against its fluctuations.

2.4 Optical set-up

The experimental setup (see Fig. 2) consisted of mounting the structure on a rotary and XY linear stages (elements 1,2) . Then TE polarized laser red light (elements 5, 12) impinged on the microcavity after passing through a mechanical chopper (element 6) and a neutral filtering wheel (3) so the electromagnetic forces can be created and the structure started moving. The movement of the microcavity was measured by a very sensitive vibration meter (elements 7,9,11). A positive loop formed by the movement measured signal, provided by the vibration meter processed through an Schmitt Trigger circuit, which output controls the pumping laser and chopper. That is when the structure started moving, immediately the circuit blocked the laser light by mean of a chopper. Once the structure returned to the initial position it triggered the pumping laser again, and so on. Once the loop was closed the structure oscillated for a few seconds at different frequencies between 2 Hz and 50 Hz. After that period the structure showed a clear trend to stabilize the self-oscillation. Typical frequencies ranged from 15 Hz to 17 Hz and from 30 Hz to 34 Hz with a duty cycle of 52%. At this frequency the movement presented a more pure spectrum with a narrow frequency spread and the structure was stable for as long as 5 minutes. We chose a Schmitt Trigger circuit based on an operational amplifier. By doing so, we have a wide range of parameters to adjust the circuit performance, and a high-speed loop reaction in reference to the mechanical deformation of the structure. The Schmitt Trigger compared the velocity signal voltage of the vibration meter with a reference voltage. The resulting electric pulsed signal controlled the chopper. By means of the oscilloscope and a photocell (elements 8,10), we verified the signal and we could recognize the desired pulses of ∓ 5 VDC and the presence of a 60 Hz signal component (some millivolts induced from the power line). We did not filter this *noise* of 60 Hz because it is useful to excite the loop because it helps to break the inertia. Otherwise, we excited the circuit by interrupting the pumping beam pass (manually) at a frequency of 2 to 3 Hz. This maneuver started the oscillation at that low frequency which is soon increased until reaching its stable oscillation mode, as said, around an average value of 16 Hz or 32 Hz. In order to prevent undesirable reflection signals enter to the vibration meter we used an infrared band-pass filter (780 nm).

Since optomechanics is related to power, we provide evidence of the influence of incident power on the observed self-oscillations of the photonic structure. Once the self-oscillation was established power levels were changed (8.3 mW, 4.5 mW, 2.6 mW and 1 mW) and the velocity PSD was measured.

2.5 Mechanical properties measurements

We used a beam loaded at end configuration for mechanical measurements. The PSi-1DPC was mounted over a glass substrate, which was attached to an XYZ stage. The sam-

ple length L was 1 mm, width b was 1.425 mm and thickness t was 7.61 microns approximately. The load force was provided by means of a lever arm. Initially the lever was at equilibrium then we added a series of known weights of $w_1 = 0.007849gr$, $w_2 = 2w_1$ and $w_3 = 3w_1$. The weights were placed at 8 mm from the lever center. Since the arm length was 216 mm we could find the load at edge as $F_i = w_i/(216/8) = w_i/27$. Then we measured mechanical displacements δ induced by the loads with a CCD camera plus an optical objective (focal length 8 mm). The optical system had a magnification of 1700 approximately.

3 Theoretical models and simulations

3.1 Electromagnetic forces calculation

There are two components of the electromagnetic force in the configuration shown in Fig. 1c [19]. One in the normal direction (perpendicular to the structure interfaces) and the second in the tangential direction (parallel to the structure interfaces). However if all dielectric layers are considered lossless layers (no light absorption) then the normal component of the force is the only one present. The mathematical expression for the normal surface force density was calculated before [10, 11] and is given by:

$$\begin{aligned}\langle F_x\rangle_T = &\sum_{l=1}^{N}\frac{\varepsilon_0}{4}\left[\left(\frac{n_{l-1}}{n_l}\right)^4-1\right]\\ &\left[\begin{array}{l}|A_l|^2+|B_l|^2+\\ 2\,|A_l|\,|B_l|\cos\left(2k_l d_l+\varphi_{A_l}-\varphi_{B_l}\right)\end{array}\right]+\\ &\frac{\varepsilon_0}{4}\left[\left(\frac{n_N}{n_s}\right)^4-1\right]\left[\begin{array}{l}|A_s|^2+|B_s|^2+\\ 2\,|A_s|\,|B_s|\cos\left(\varphi_{A_s}-\varphi_{B_s}\right)\end{array}\right]+\\ &\sum_{l=1}^{N}\frac{\varepsilon_0}{2}\left[(n_l)^2-1\right]|A_l|\,|B_l|\left[\begin{array}{l}\cos(\varphi_{A_l}-\varphi_{B_l})-\\ \cos\left(2k_l d_l+\varphi_{A_l}-\varphi_{B_l}\right)\end{array}\right],\end{aligned} \tag{1}$$

where ε_0 is the vacuum permittivity and N is the total number of layers.n_i are the refractive indices of the layers or substrate, k_i and d_i are the wavenumbers and thicknesses of the layers respectively. The complex amplitudes A_i's and B_i's and their phases φ_i can be calculated by using the well-known transfer matrix method [20] for 633 nm, angle of incidence of 35 degrees, TE polarization and irradiance level of 13 mW/3 mm^2. The two first terms in Eq. 1 are originated at the interfaces between the dielectric layers, where polarization surface charge is created, giving rise to a surface force density. The last term is due to the Lorentz volume force density integrated within each dielectric layer.

3.2 Electromagnetic forces simulation

We performed full-wave finite element simulations (FEMLAB 3.1) at 633 nm (irradiance level of 13 mW/3mm^2) for TE polarization light considering the experimental thickness we found and refractive indices we inferred from the band structure fitting (optical losses were neglected). The incidence angle was 35 degrees. The mesh was created with 70 nm triangles and numerical tolerance of 10^{-6}. The simulation outputs are electromagnetic fields whereby electromagnetic forces are calculated.

First, in order to show the importance of using PCs on electromagnetic force generation, we simulated a structure (structure I) consisting of an homogeneous PSi dielectric slab with refractive index of 1.1 (n_1 in our 1DPC), an air-gap of 9 microns and again the homogeneous PSi dielectric slab with refractive index of 1.1. Second, we simulated a structure (structure II) having a 1DPC with 10 periods, an air –gap of 9 microns and again a 1DPC with 10 periods. The total thickness for both structures was the same and the period for structure II is the same as the experimental period.

3.3 Mechanical model for self-oscillations

The simplest self-oscillating system can be represented as consisting of a constant source of energy, a mechanism regulating the supply of energy to the oscillating system, and the oscillating system itself. An essential feature of such a system is its feedback nature: on the one hand, the regulating mechanism controls the motion of the oscillating system but, on the other, it is the motion of the oscillating system that influences the operation of the regulating mechanism [12].

An example of a very simple oscillating system that can produce either self or forced oscillations is a pendulum in a viscous frictional medium acted upon by a force of constant magnitude. The differential equation of this dynamical system is

$$\begin{aligned}&\ddot{x}+2h\dot{x}+\omega_0^2 x=\langle a_x\rangle_T \qquad jT<t<(n_{force}+j)T\\ &\ddot{x}+2h\dot{x}+\omega_0^2 x=0 \qquad (n_{force}+j)T<t<(j+1)T\\ &j=0,\ldots m\end{aligned} \tag{2}$$

where, $\langle a_x\rangle_T = \langle F_x\rangle_T A_{eff}/m_{PSi-1DPC}$, A_{eff} is the effective surface area covered by the light beam h is a damping coefficient, ω_0 is the natural frequency of the system, n_{force} defines the duty cycle (fraction of the period where the force is on) which should take a value of 0.5 for the self-oscillation case and $j+1$ is the number of cycles that the force is on and off. A typical property of all self-oscillating

systems is the connection between the constant source of energy and the system, which is such that the energy given by the source varies periodically, the period of this variation being determined by the properties of the system. In this case, the period T is related to the oscillator's frequency ω as usual by $T = 2\pi/\omega$ and it is related to the natural frequency and damping coefficient as $\omega^2 = \omega_0^2 - h^2$. So, in Equation 1, T, n_{force}, A_{eff} and $m_{PSi-1DPC}$ are known parameters from the experiment and $\langle a_x \rangle_T$ from theoretical calculations and computer simulations. Parameters ω_0 and h can be known by the self-oscillation condition.

3.3.1 Self-oscillation condition

The self-oscillation condition arise, in principle, in the following manner. Consider Fig. 2, there the energy is provided by a polarized laser light (elements 5, 12) and a chopper (element 6). Initially, when the light is on, the electromagnetic force pushes down the structure (descending part). Now suppose that the energy dissipated throughout this part of the period is compensated by energy from the laser-chopper, since it is only then when the laser is in effective operation. If the compensation is exact in this part of the period, i.e., if there is neither a gain or loss of energy, a prolonged oscillation will be reached. That is to say, the system will go into a steady oscillatory state with period T. In the second part of the period, the structure naturally goes into a damped oscillation until it stops and returns to the original position (ascending part). Mathematically, we can calculate this condition as $\left|2h\int_0^{T/2}\dot{x}^2dt\right| = \left|\int_0^{T/2}\langle a_x\rangle_T\,\dot{x}dt\right| = \left|\int_0^{T/2}\langle a_x\rangle_T dx\right|$ for $t \in [0, T/2]$, we can approximate this condition, without knowing the exact solution of equation 1, by using the maximum values for the displacement x_p and velocity V_p. Therefore the self-oscillation condition reads

$$\left|2hV_p^2T/2\right| = \left|\langle a_x\rangle_T x_p\right|. \tag{3}$$

Therefore by knowing V_p ,x_p and $\langle a_x\rangle_T$ the parameter h can be calculated and from $\omega^2 = \omega_0^2 - h^2$ the parameter ω_0 is estimated.

3.3.2 Doubling the self-oscillation frequency

Since the upper component of the PSi-1DPC structure can be considered as a mechanical beam and due that one edge of the beam is clamped and the other edge is not completely free (when light is on the force push both 1D-PCs and when it is off they are released) then the best configuration should be a hinged-clamped beam. It is well known that for a hinged-clamped beam the natural frequencies are:

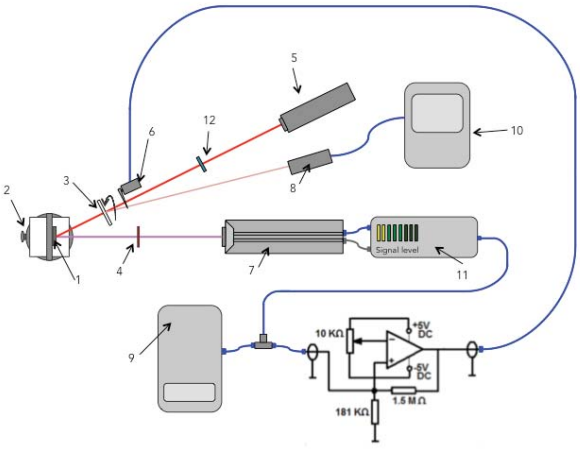

Figure 2: Self-oscillation experimental configuration. 1 Porous silicon microcavity structure, 2 Rotary and linear XY stages, 3 Neutral filter wheel, 4 Infrared band-pass filter, 5 He-Ne laser, 6 Mechanical chopper, 7 Vibration meter laser, 8 Photocell, 9 Computer, 10 Oscilloscope, 11 Vibrometer interface, 12 Linear polarizer. The circuit shown represents a Schmitt Trigger.

$$\omega_{0i} = \alpha_{0i}^2\sqrt{\frac{EI}{\mu L^4}}, \tag{4}$$

where E is the beam's Young modulus, I is the second moment of area of the beam's cross section. μ is the mass density per unit length, L is the beam's length and α_{0i} are constants whose values depend on the boundary conditions. In this case the values for the fundamental frequency and first harmonic are $\alpha_{01} = 3.924283374$ and $\alpha_{02} = 7.071067812$. This implies that both natural frequencies are separated by $\omega_{02} = \omega_{01}(\alpha_{02}/\alpha_{01})^2 = 3.246753247\omega_{01}$.

Since we are doubling the self-frequency thus $\omega_2 = 2\omega_1$ with $\omega_i^2 = \omega_{0i}^2 - h_i^2$. Clearly if we know the values for ω_1, ω_{01} and h_1 we can calculate the values for ω_{02} and h_2 and then use these values in Eq. 2 and simulate it.

3.4 Young's modulus and Stiffness estimations

From Eq. 4 Young's modulus can be estimated from the fundamental natural frequency ω_{01} as $E = \omega_{01}^2\mu L^4/\alpha_{01}^4 I$ with $I = bt^3/12$ and $\mu = \rho_{PSi-1DPC}bL$. Where b is the width, t is the thickness, and $\rho_{PSi-1DPC}$ is the volumetric

density of the PSi-1DPC. The stiffness k can be calculated as $\omega_{01} = \sqrt{\alpha_{01}^4 EI/(\mu L)L^3} = \sqrt{\alpha_{01}^4 EI/mL^3} = \sqrt{k/m}$ where m is the mass. Therefore $k = \alpha_{01}^4 EI/L^3$.

Mechanically it is known that the relationship between stiffness and Young's modulus in a cantilever beam loaded at the end is given by $k = F/\delta = 3EI/L^3$. Thus by knowing k is possible to know E and viceversa.

4 Results

4.1 Electromagnetic forces

From Eq. 1 and computer simulations we calculated the electromagnetic force induced within structures I and II over a surface area of 3 mm^2. For structure I the theoretical electromagnetic force magnitude was 48 pN. The computer simulation gave a force magnitude of 7.2 pN. For structure II the theoretical force magnitude was 6.36 nN and the computer simulation force magnitude was 6.20 nN. In Fig. 3a we observe the electromagnetic field distribution within structure I and in Fig. 3b for structure II. Fig. 3c and 3d shows the volume electromagnetic force density for structures I and II respectively. Finally Fig. 3d shows the surface electromagnetic force density for structure I and II respectively. By integrating the volume electromagnetic force density along each dielectric layer we obtained the Lorentz contribution to the surface electromagnetic force density. It is clear from both structures that the layer that contributes the most to the force density is not the air-gap region.

Fig. 4a shows the harmonic variation of the surface force density with the air-gap length for structure II. We can observe that this force density oscillates between values of 2 and 3.5 mN/m^2 (6 and 10.5 nN for a surface area of 3 mm^2) for air-gaps lengths ranging from 10 nm up to more than 1 mm. Fig. 4b shows the harmonic variation of the surface force density with the air-gap length for structure I. We can observe that this force density oscillates between values of 0.015 and 0.03 mN/m^2 (45 and 91 pN for a surface area of 3 mm^2) for air-gap lengths ranging from 10 nm up to more than 1 mm. In both cases we could not see any resonance state due to a localized state.

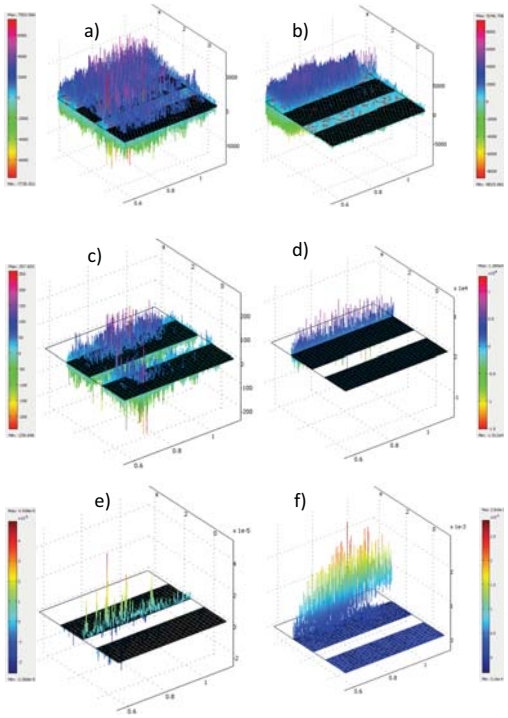

Figure 3: a) Electromagnetic field distribution within structure I. b) Electromagnetic field distribution within structure II. c) Volume electromagnetic force density distribution within structure I. d) Volume electromagnetic force density distribution within structure II. e) Surface electromagnetic force density distribution within structure I and f) Surface electromagnetic force density distribution within structure II. Clearly both force densities are bigger within structure II than within structure I.

4.2 Role of laser fluctuations or mechanical vibrations introduced by external factors on self-oscillations origin

We did not find any self-oscillation frequency under the two control experiments. What we found in both cases was a clear $1/f^{\epsilon}$ noise spectrum as is depicted in Fig. 5a-b. In Fig. 5c we observe a typical self-oscillation light waveform. Cleary the jitter caused by the laser fluctuations are small compared with the light waveform amplitude.

4.3 Self-oscillations experiments

In Fig. 6, we observe three typical examples of the experimental structure velocity time series, where we can see an asymmetry between the descending (positive voltage) and the ascending (negative voltage) parts, implying that

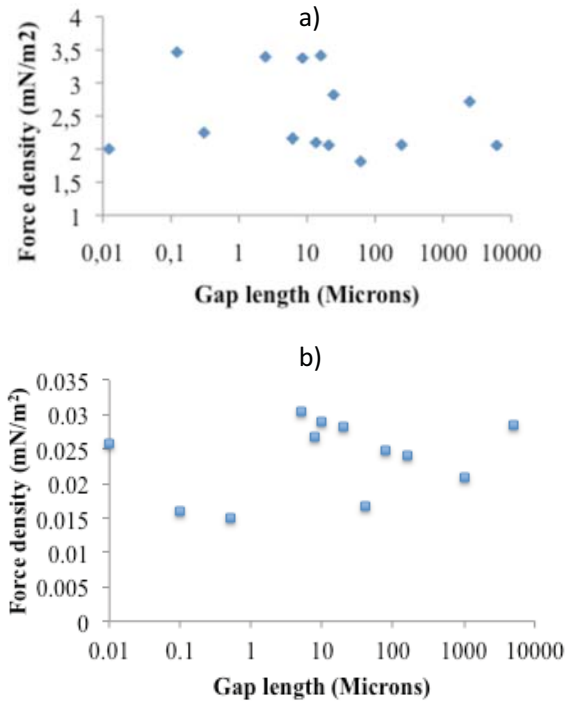

Figure 4: a) Theoretical surface force density (Eq. 1) at different air-gap lengths in structure II. The surface density force oscillates between 2 and 3.5 mN/m^2 with gap lengths of more than 1 mm and b) Theoretical surface force density (Eq. 1) at different air-gap lengths in structure I. The surface density force oscillates between 0.015 and 0.03 mN/m^2 with gap lengths of more than 1 mm.

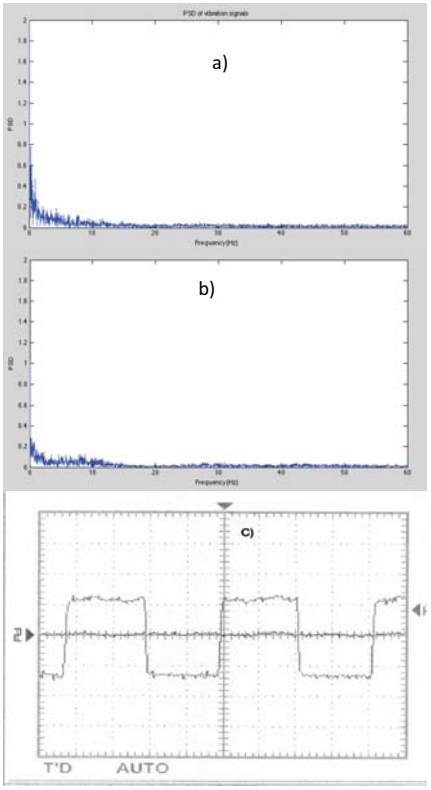

Figure 5: a) Role of mechanical vibrations introduced by external factors on self-oscillations origin. Vibrations were measured in the photonic structure during 5 minutes. No peaks are observed in the PSD meaning that external vibrations cannot produce self-oscillations. b) Role of laser fluctuations introduced by external factors on self-oscillations origin. Vibrations were measured in the photonic structure with the laser on during 5 minutes. No peaks are observed in the PSD meaning that laser fluctuations cannot produce self-oscillations either. c) By means of an oscilloscope and a photocell, we verified the light signal waveform and duty cycle after the light beam was chopped. This control helped to compare the light signal waveform against its fluctuations. As we can observe laser fluctuactions are small compared with the waveform amplitude.

the damping coefficient of the descending part is higher than the coefficient of the ascending part. Fig. 6a shows the onset of self-oscillations, this happens once the loop was closed and the structure oscillated for a few seconds at different frequencies between 2 Hz and 50 Hz. Fig. 6a-I shows the structure velocity signal and Fig. 6a-II its corresponding power spectral density. Once the self- oscillations were established the structure velocity signal (Fig. 6-b) tended to stabilize the self-oscillation at 16 Hz (Fig. 6b-II) with a duty cycle of 52%. We found experimental values for x_p = 4.12 microns and V_p = 0.42 mm/s. In some cases after the stable 16 Hz self-oscillation interval the structure could double its self-oscillation frequency as it is shown in Fig. 6c, that is 32 Hz with an amplitude of 3.838 microns and velocity of 0.7 mm/s. In another experiment while the photonic structure self-oscillated at 17 Hz we decreased the power from 8.3 mW to 1 mW. We noticed a clear frequency peak for 8.3 mW power level and its onset at 4.5 mW. Below that value the peak was embedded within the noise floor and we took the highest frequency peak noise as a marker to compare against self-oscillation peaks when presented. Fig. 6d shows the result.

4.4 Self-oscillations model

4.4.1 Structure II

4.4.1.1 Oscillation of 16 Hz

In order to use the self-oscillation theoretical model we have to estimated the parameters $\langle a_x \rangle_T$, h and ω_0. We can estimate the parameter $\langle a_x \rangle_T$ as follows: Since experimen-

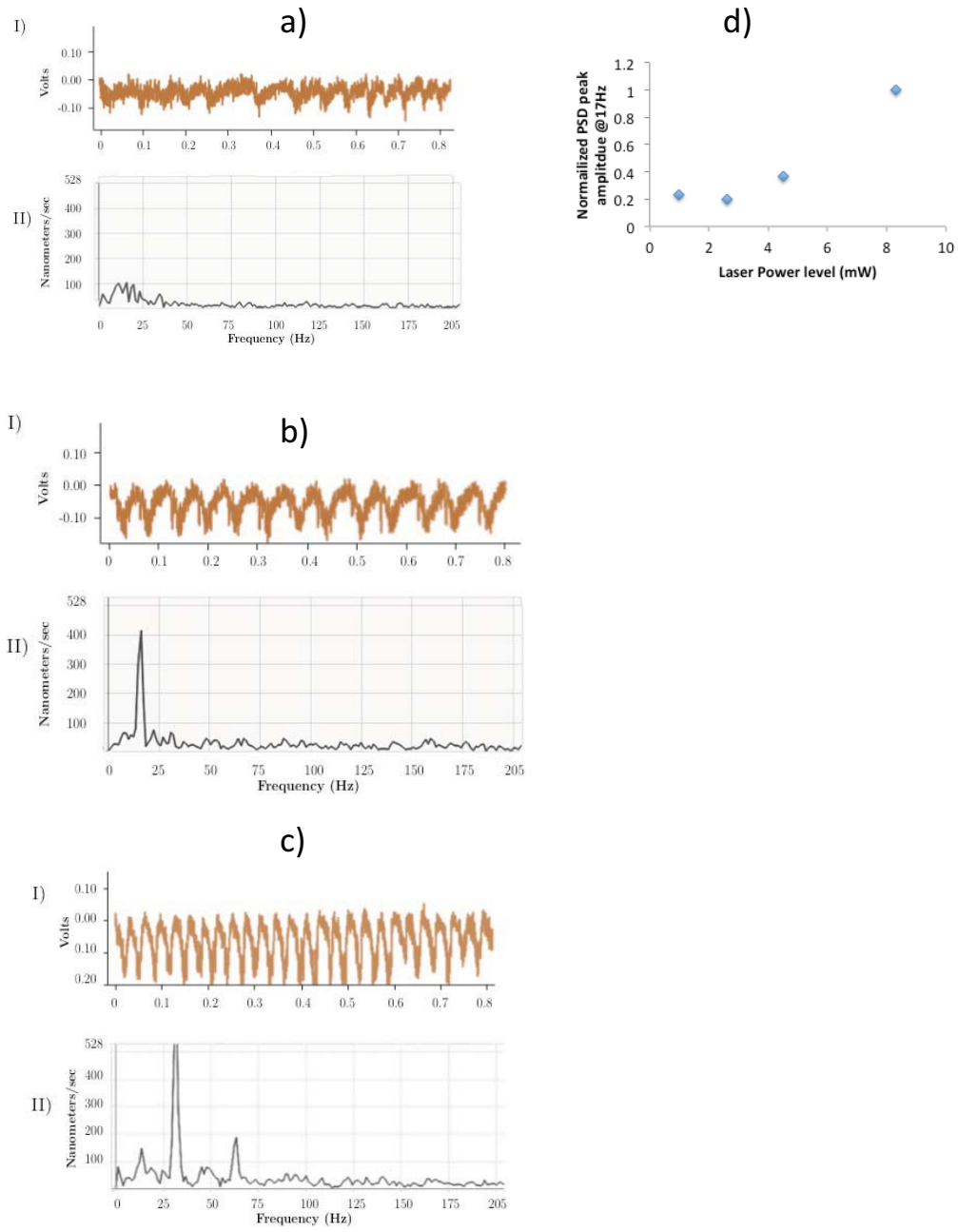

Figure 6: Self-oscillations experimental results. a) I) Experimental velocity time series. II) Experimental power spectral density for the velocity. In this case, we observed the self-oscillation onset. b) I) Experimental velocity time series. II) Experimental power spectral density for the velocity. Here the self-oscillation was stable up to 5 minutes at frequency of 16 Hz. c) I) Experimental velocity time series. II) Experimental power spectral density for the velocity. We can see that the frequency of self-oscillation is 32 Hz. The stability last less than the previous case. d) Influence of incident power on the observed self-oscillations of the photonic structure. While the photonic structure self-oscillated at 17 Hz we decreased the power from 8.3 mW to 1 mW.

tally we have no control on the air-gap, we took the average value between the maximum and minimum values for $\langle F_x \rangle_T$ that equals 2.75 × 10^{-3} N/m^2 and since A_{eff} = $\pi \times 10^{-6} m^2$ and $m_{PSi-1DPC}$ =3.57 × 10^{-8} kg the value for $\langle a_x \rangle_T$ is 0.242 m/s^2. According with the values obtained for x_p, V_p, T and $\langle a_x \rangle_T$ we found that the self-oscillation condition (Eq. 4) gave a value for h of 91.1 and from there ω_0 = 136.1118.

We simulated Eq. 2 by using Matlab and the best fit we found uses the aforementioned parameters and only the parameter h needed to be multiplied by 15 instead of 2 in the descending part and we use the experimental value n_{force} = 0.52 . Figures 7a–b shows the simulated velocity time series and its PSD. In order to take into account uncontrollable vibration effects, 60 Hz noise, etc. we added a zero-mean random noise to the simulated velocity time series. The amplitude of this noise signal was 25% of the peak velocity amplitude. The maximum displacement value was 4.146 microns, which is of the same order of magnitude that the experimental value.

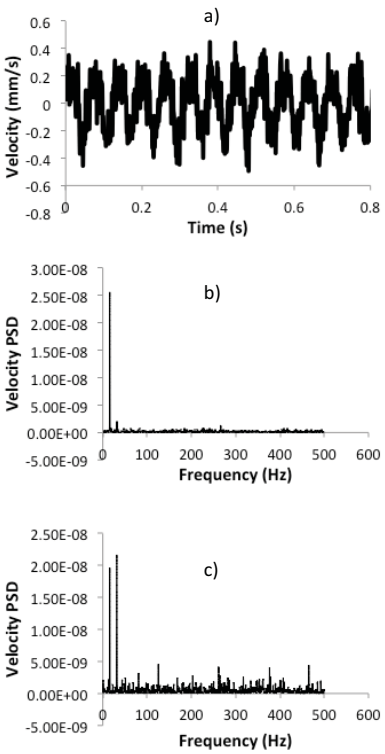

Figure 7: Self-oscillation at 16 Hz theoretical results. a) Theoretical velocity time series. (b), Theoretical power spectral density for the velocity at 52% duty cycle. (c) Theoretical power spectral density for the velocity at 65% duty cycle. A second peak at 32 Hz appeared.

4.4.1.2 Oscillation of 32 Hz

In section 3.2.2 we found that ω_{02} = 3.246753247ω_{01} and since ω_2 = 2π(32) we found a value for ω_{02} = 441.9214 and h_2 = 394.49092. We simulated Eq. 2 as before and we used the experimental value n_{force} = 0.52 again. Figures 8a–b shows the simulated velocity time series and its PSD. Again we added a zero-mean random noise to the simulated velocity time series with maximum amplitude of 25% of the peak velocity amplitude. The maximum displacement value was 1.6 microns, which is of the same order of magnitude than the experimental value.

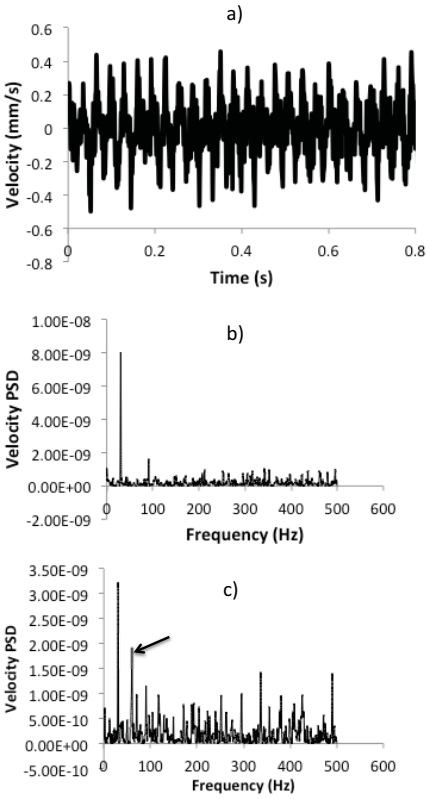

Figure 8: Self-oscillation at 32 Hz theoretical results. a) Theoretical velocity time series. (b), Theoretical power spectral density for the velocity at 52% duty cycle. (c) Theoretical power spectral density for the velocity at 65% duty cycle. A second peak at 64 Hz appeared (mark by the arrow).

4.4.1.3 Oscillation of 64 Hz

In Fig. 6c besides the 32 Hz peak, there is a peaks at 64 Hz by using the same parameters as in the precedent section except for n_{force} both peaks can be simulated. The 64 Hz peak appears along with the 32 Hz peak when n_{force} value

is around 65%. The simulated peaks can be seen in Fig. 8c as well.

4.4.2 Self-oscillations in structure I

We used Eq. 2 along with the magnitude of the force found in section 4.1 to see whether structure I self-oscillates. As before we estimated the parameter $\langle a_x \rangle_T$, we took the same volume value as the one presented in section 2.2 which had a value of 6.09×10^{-11} m^3. The volumetric density of each homogeneous PSi slab was (1–0.88) × 2330 kg/m^3 that equals 279.6 kg/m^3. Multiplying the volume times the effective volumetric density gave us a mass of 1.70276×10^{-8} kg. Since experimentally we have no control on the air-gap we took the average value between the maximum and minimum values for $\langle F_x \rangle_T A$ that equals 68 pN thus the value for $\langle a_x \rangle_T$ was 0.00399351 m/s^2. Assuming the same h_1 and ω_{01} as in structure II we obtained $x_p = 55$ nm. Clearly we do not expect to measure any self-oscillation peak at all for our current experimental conditions, if there is a peak then it should be embedded within the noise floor.

4.5 Young's modulus and Stiffness estimations

By using parameter values given before for b, t,L, μ = 0.004688 kg/m, and ω_{01} = 136.1118 we found $I = 7.3452\ 10^{-10} m^4$, $E = 1.28\ GPa$ and $k = 0.3474\ N/m$. From our mechanical measurements we obtained $F_1 = 2.8506\ 10^{-5} N$, $d_1 = 4.97577\ 10^{-5} N$, $F_2 = 5.7013\ 10^{-5} N$, $d_2 = 8.95638\ 10^{-5} N$, $F_3 = 8.5519\ 10^{-5} N$, $d_3 = 12.2345\ 10^{-5} N$. We plotted (not shown) the load force vs. displacements and fit the curve with a straight line. We obtained a good linear fit with a coefficient of determination (R^2) of 0.97251. The value for k (represented by the slope) had a value of 0.6671 N/m. From here we can calculate Young's modulus by using $k = F/\delta = 3EI/L^3$. Using the parameter values presented in section 2.3, the value of k = 0.6671 N/m, we found that $I = 5.2334 \times 10^{-20}$m^4 and $E = 4.25\ GPa$.

5 Discussion

Normally optical characterization of a microcavity or any photonic resonator is essential before undertaking or proving any experimental effects related to optomechanics and optical forces. However we have shown in Fig. 4 that there are no localized states for a wide range of air-gaps values at 35 degrees. This is not the case for the same structure but at normal incidence as we have shown in [11]. Nonetheless even when the incident laser wavelength does not match the resonance wavelength of the PSi-1DPC microcavity (structure II) there is a considerable electromagnetic force generation that can produce mechanical oscillations. Moreover, in order to prove the oscillations are indeed due to the generation of optical forces within the whole photonic structure. A control sample (structure I) with the same porous silicon thickness for each half, separated by an air-gap was simulated. In fact the light induced a surface force density in structure I but it is two orders of magnitude lower than the one induced in structure II. This is true for a wide range of air-gap lengths from nm to mm. This means that structure I could oscillate with amplitude of 55 nm. Such amplitude will be impossible to measure with our current experimental setup and we do not expect any peak in the PSD. Just to compare the force magnitude generated within structure I it is of the same order of magnitude to the force generated (100 pN @43 mW) in a polystyrene sphere with a mass of 4 ngr [21]. Further, other factors that could induce 16 Hz and 32 Hz oscillations could be fluctuations in laser power and mechanical vibrations introduced by the setup, building or enviroment. Nevertheless our control experiments, showed otherwise, where we measured vibrations on structure II for 5 minutes without laser light and 5 minutes with laser light. In both cases we did not observe any specific peak frequency on the PSD. A clear $1/f^{\varepsilon}$ noise spectrum was observed in both cases.

Experimentally we found self-oscillations at 16 Hz, 32 Hz and possibly at 64 Hz. Experimentally the duty cycle was 0.52. The reason why the duty cycle does not change when the structure switches from 16 Hz to 32 Hz is due that the self-oscillation condition is still fulfilled. That is all the elements mechanical (chopper), electronics (Schmitt trigger), optical (vibration meter), etc., that contribute to create self-oscillations are fast enough to sustain the condition that gain equals losses in half-cycle. We provided evidence of the influence of incident power on the observed self-oscillations of the photonic structure. Incident power versus PSD peaks gave a laser-like behavior meaning that there is a threshold point where the gain equals the losses. This unveils that the self-oscillation condition is a necessary condition but is not sufficient. We also proved that there are no fluctuations in laser power that may interfering with the observed oscillation frequencies. This has been done by measuring laser powers after the chopper (component 8 in Fig. 2). Laser power fluctuations were

small compared with waveforms created by the mechanical chopper.

Theoretically, the photonic structure can be seen as a hinged-clamped beam with their natural frequencies separated by unequal factors. For instance the fundamental frequency and the first harmonic are separated by a factor of 3.25. The 16 Hz self-oscillation begin at a frequency close to the fundamental frequency due to the losses. If the losses change then the self-oscillation frequency changes accordingly. Then as long as the gain is equal or bigger than the losses the 16 Hz self-oscillation is maintained but when the duty cycle changes to 65% a 32 Hz frequency peak with approximately the same amplitude as the 16 Hz frequency appears (Fig. 7c). This means that the photonic structure could switch from the natural fundamental frequency to its first harmonic creating the 32 Hz self-oscillation. Once the 32 Hz self-oscillation has been established its dynamics is similar as before because we can see on the PSD the appearance of the 64 Hz peak (Fig. 8c). This means that the photonic structure spend some time oscillating at 32 Hz close to a duty cycle of 50% and suddenly it could oscillates with a higher duty cycle of 65%. This last duty cycle permits the chopper create a waveform that contains both the 32 Hz and 64 Hz frequencies but the 64 Hz frequency PSD peak amplitude is much lower than the 32 Hz thus the switching from 32 Hz to 64 Hz is not possible. From this result, we can conclude that the photonic structure is not able to self-oscillate at 64 Hz.

We have estimated the photonic structure stiffness and Young's modulus with data obtained from the self-oscillation experiments and from a mechanical experiment. From the self-oscillation method we found that $k = 0.3474$ N/m and $E = 1.28$ GPa. From our mechanical measurements we obtained $k = 0.6671$ N/m and $E = 4.25$ GPa. In [22] Young's modulus for PSi layers are reported for different porosities and substrate conductivities. Since each PSi-1DPC contains two different porosities therefore there are two different Young's modulus. In order to obtain an effective Young's modulus, we can take a weight average of both modulus where the weights correspond to each thickness fraction. For PSi layers with porosities of 65% and 88% the Young modulus are 14.66 GPa and 1.69 GPa respectively then the effective Young's modulus should be 9.10 GPa. This value is bigger than the ones we obtained by our optical or mechanical experiments but we have to bare in mind that values reported in [22] were obtained on PSi layers that were not lifted off from the crystalline silicon substrate. A fact that may influence Young's modulus determination. Herein the Psi-1DPCs are free standing samples with no influence from any substrate.

6 Conclusions

We experimentally induced self-oscillations in a microcavity structure made of porous silicon one-dimensional photonic crystals (1DPC) with an air-gap. We found self-oscillations frequencies of 16 Hz and 32 Hz in our photonic structure. In order to induce self-oscillations it is not necessary that any resonance wavelength of the photonic structure matches the incident laser wavelength (633 nm) as we showed by theory, computer simulations and experiments. However from a practical point of view a better optical optimization of the PSi-1DPC structure should be done before attempting any device fabrication. PSi mechanical properties were estimated from the self-oscillation experiments and from mechanical experiments. The Stiffness and Young's modulus values were of the same order of magnitude that the ones reported on the literature by other methods.

Acknowledgement: This work was supported by an NSERC Discovery operating grant. N.S.C. wants to thank to CONACYT for the scholarship "Beca Mixta-Movilidad en el Extranjero". M.A.P.O. would like to thank to magnetophotonics material SEP-PRODEP grant. M.B. de la Mora thanks to the financial support of Chairs program from CONACYT and PAPIIT IT2013 from UNAM. We would like to thank the photonic systems group at McGill University for providing software for the simulations.

References

[1] De Stefano, L., Moretti, L., Lamberti, A., Longo, O., Rocchia, M., Rossi, A. M. and Rendina, I, Optical sensors for vapors, liquids, and biological molecules based on porous silicon technology, IEEE. T. Nanotechnol., 2004, 3.

[2] Torres-Costa, V. and Martin-Palma, R. J, Application of nanostructured porous silicon in the field of optics. A review, J. Mater. Sci., 2010, 45.

[3] J. D. Joannopoulos, S. G. Johnson, J. N. Winn, and R. D. Meade, Photonic Crystals Molding the Flow of Light, Princenton University Press, Princeton and Oxford, 2008.

[4] J. E. Lugo, H. A. Lopez, S. Chan and P. M. Fauchet, Porous silicon multilayer structures: a photonic band gap analysis, J. Appl. Phys., 2002, 91.

[5] Y. Fink, J. N. Winn, S. Fan, C. Chen, J. Michel, J. D. Joannopoulos, and E. L. Thomas, A dielectric omnidirectional reflector Science, 1998, 282.

[6] V. Agarwal, J. A. del Río, G. Malpuech, M. Zamfirescu, A. Kavokin, D. Coquillat, D. Scalbert, M. Vladimirova and B. Gil, Photon Bloch oscillations in porous silicon optical superlattices, Phys. Rev. Lett., 2004, 92.

[7] J. O. Estevez, J. A. Arriaga, A. Mendez-Blas, E. Reyes-Ayona, J. Escorcia, and V. Agarwal, Demonstration of photon Bloch oscillations and Wannier-Stark ladders in dual-periodical multilayer structures based on porous silicon, Nanos. Res. Lett., 2012, 7.
[8] G. A. Rodriguez, J. L. Lawrie, and S. M. Weiss, H. A. Santos (Ed.), Porous silicon biosensors for DNA sensing, Porous Silicon for Biomedical Applications, Woodhead Publishing Ltd., 2014.
[9] J. E. Lugo, R. Doti, and J. Faubert, Negative refraction angular characterization in one-dimensional photonic crystals, PLoS ONE, 2011, 6.
[10] J. E. Lugo, R. Doti, N. Sanchez, M.B. de la Mora, J.A. del Rio and J. Faubert, The bifoil photodyne: a photonic crystal oscillator, Sci. Rep., 2014, 4.
[11] J. E. Lugo, J, R. Doti, N. Sanchez and J. Faubert, Inducing forced and auto-oscillations in one-dimensional photonic crystals with light, J. Nanophotonics., 2014, 8.
[12] A. A. Andronov, A. A. Vitt and S. E. Khakin, Theory of Oscillators, W. Fishwick NY, 1987.
[13] A. V. Panfilov, R. H. Keldermann and M. P. Nash, Self-organized pacemakers in a coupled reaction-diffusion-mechanics system, Phys. Rev. Lett., 2005, 95.
[14] P. Kohl, P. Hunter and D. Noble, Stretch-induced changes in heart rate and rhythm: clinical observations, experiments and mathematical models, Prog. Biophys. Molec. Biol., 1999, 71.
[15] A. Jenkins., Self-oscillation, Phys. Rep., 2013, 525.
[16] Yoshida, R., Takahashi, T., Yamaguchi, T. and Ichijo, H., Self-oscillating gel. J. Am. Chem. Soc., 1996, 118.
[17] Yoshida, R. and Ueki, T., Evolution of self-oscillating polymer gels as autonomous polymer systems. NPG Asia Mater., 2014, 6.
[18] Nava, R., de la Mora, M. B., Taguena-Martinez, J. and del Rio, J. A. Refractive index contrast in porous silicon multilayers, Phys. Status. Solidi. C., 2009, 6.
[19] Mizrahi, A., Optical bragg accelerators, Phys. Rev. E., 2004, 70.
[20] Pochi Yeh, Optical waves in layered media, Wiley and Sons, 2005.
[21] Li, Y., Svitelskiy, O. V., Maslov, A. V., Carnegie, D., Rafailov, E. and Astratov, V. N. Giant resonant light forces in microspherical photonics, Light. Sci. Appl., 2013, 2.
[22] Canham, L., Handbook of Porous Silicon, Springer, 2014.